nature communications

Article

https://doi.org/10.1038/s41467-025-57815-5

Miniature origami robot for various biological micromanipulations

Received: 26 May 2024

Accepted: 27 February 2025

Published online: 17 March 2025

Check for updates

Bo Feng [1,2,3,4,6], Yide Liu [1,2,3,4,6] ✉, Jiahang Zhang [1,2,3,4,6], Shaoxing Qu [1,2,3,4,5] ✉ & Wei Yang [3,4]

Robotic micromanipulation is widely applied in biological research and medical procedures, providing a level of operational precision and stability beyond human capability. Compared with traditional micromanipulators that require assembly from many parts, origami manipulators offer advantages such as small size, lightweight, cost-effectiveness, and scalability. However, there are still requirements in biological application to address regarding stiffness, precision, and dexterity. Achieving a compact and functional parallel mechanism through origami structures remains a challenging problem. Here, we present the Micro-X4, a 4-Degree-of-Freedom (4-DoF) origami micromanipulator, which offers a workspace of 756 mm^3, with a precision of 346 nm and a stiffness of 2738 N/m. We conduct a series of micromanipulation tasks, ranging from the tissue scale to the subcellular scale, including pattern cutting, cell positioning and puncturing, as well as cell cutting and insertion. Contact force measurement is further integrated to demonstrate precise control over cell operations and puncturing. We envision the Micro-X4 as the foundation for the next generation of lightweight and compact micromanipulation devices.

Micromanipulation[1] involves the manipulation of tiny objects using precision tools, and it finds wide applications in the fields of microsurgery[2], cell manipulation[3], and microassembly[4,5]. The strategies of micromanipulation can be broadly categorized as noncontact and contact methods, with field-driven and robotic manipulation[1,6,7] being typical approaches for each. Previous research has demonstrated the capabilities of robotic micromanipulation in tasks such as cell injection[3], cell characterization[8,9], grasping[10,11], and patch clamp[12]. Robotic micromanipulation involves utilizing a micromanipulator equipped with an end-effector. The micromanipulator acts as a platform for precise movements to a target location and orientation, while the end-effector interacts with objects. Micromanipulators are typically multi-DoF mechanical systems constructed from metals and actuated by motors or piezoelectric ceramics. They can seamlessly integrate with microscopes, providing a few millimeters of stroke with exceptionally high positioning resolution, generally at the submicrometer scale. However, these manipulators often have a large volume compared to their workspace, making them unsuitable for compact integration with other devices. In addition, due to structural constraints and limitations in their fabrication and assembly processes, miniaturizing these manipulators faces numerous challenges.

Origami robots[13–16] represent a novel machining method with unique advantages in manufacturing small and lightweight microrobots and micromanipulators. These technologies enable the assembly of 2-D materials into complex and compact 3-D structures through folding. This method has found successful applications in areas such as robotic insects[17,18], micromanipulators[19,20], human-machine interfaces[21], and microsurgery robots[22]. The joints of origami robots are achieved through the bending of soft beams, resembling the "living hinge" of compliant mechanisms[23]. Several classical

[1]State Key Laboratory of Fluid Power & Mechatronic Systems, Zhejiang University, Hangzhou, China. [2]Key Laboratory of Soft Machines and Smart Devices of Zhejiang Province, Zhejiang University, Hangzhou, China. [3]Department of Engineering Mechanics, Zhejiang University, Hangzhou, China. [4]Center for X-Mechanics, Zhejiang University, Hangzhou, China. [5]Eye Center of the Second Affiliated Hospital, School of Medicine, Zhejiang University, Hangzhou, China. [6]These authors contributed equally: Bo Feng, Yide Liu, Jiahang Zhang. ✉e-mail: yide_liu@zju.edu.cn; squ@zju.edu.cn

parallel mechanisms have been miniaturized using this method[19,21], resulting in micromanipulators with superior attributes, including high precision, speed, and dexterity.

However, current manipulators often find difficulties to meet all the requirements of microsurgery and cell manipulation, particularly in terms of stiffness and mobility. The origami micromanipulators have limited stiffness due to their soft joints, which makes them less suitable for equipping additional sensors or executing contact operations. Moreover, most previous origami micromanipulators had no more than three limbs, limiting their mobility to three DoFs. Increasing the number of limbs can benefit parallel micromanipulators by providing both stiffness and mobility, as they can offer more support and actuation to the moving platform, while also bringing complexity to the design of origami structures and the folding assembly processes.

Taking the Smart Composite Microstructure (SCM) method as an example, there are several limitations in the fabrication processes[24]. Firstly, all neighboring links are connected by flexible membranes, thus the structure can only contain revolute joints. Secondly, during the laser machining process, all links must be flat. These limitations bring challenges in fabricating closed-loop structures and folding structures to assemble. The molding method demonstrates its capability to manufacture parallel mechanisms with more limbs, as seen in the MiGriBot[25], a four-limb parallel micromanipulator with three translation DoFs plus a grasping DoF. However, the joints formed by this method are made of polydimethylsiloxane (PDMS), resulting in low stiffness. To meet the mobility and stiffness requirements in micromanipulation while ensuring operational precision and workspace, we identify and address two major challenges: developing origami parallel micromanipulators with more limbs and DoFs and achieving driving and control strategies to maximize the actuation precision.

Here, we present the Micro-X4, a four-limbed origami parallel manipulator with four DoFs, including three translational DoFs and one rotational DoF along the central axis of its moving platform. The mechanism of the Micro-X4 was proposed originally for high-speed pick-and-place manipulation[26,27]. The Micro-X4 offers a substantial workspace of 756 mm^3 for constant-orientation and 362 mm^3 for total orientation, with a sub-micron precision of 346 nm and a stiffness of 2738 N/m.

To fabricate the Micro-X4, we propose a strategy for achieving the complex origami parallel mechanism, which we called “split and splice”(see Methods section ‘The “split and splice” method’ and Supplementary materials Note. S1). We have shown the universality of this method in fabricating various types of closed-loop parallel mechanisms through the SCM method. The “split and splice” approach can expand the scope of the SCM method and provide more devices in the field of micromanipulation. To control the Micro-X4, we propose the analytical kinematic solution considering the characteristics of the origami structure (see Methods section ‘Kinematic model’ and Supplementary materials Note. S4).

We have demonstrated the micromanipulation capabilities of the Micro-X4 with several examples. The Micro-X4 is capable of performing tasks such as: (1) Cutting out patterns on the surface of the onion. (2) Locating the cell nucleus in onion slices and puncturing onion cells. (3) Utilizing the rotational DoF of the moving platform to switch the end-effectors, enabling the cutting and inserting of a cabbage cell. (4) Integrating contact force measurement enables precise cell touching and puncturing.

Results

System description

Our micromanipulator contains an origami parallel mechanism with four limbs, which has four DoFs - the translations along the X, Y, and Z-axis and the rotation along the Z' axis of the moving platform (Fig. 1b and Supplementary video. S1). The rotational DoF enables the robot to control the orientation of the blade as an end-effector during the pattern cutting or to switch the end-effectors to achieve complex tasks (Fig. 1e and f). We further perform the rotational capability with a simplified example. The Micro-X4 can insert the cube into the eight-pointed star-shaped holes with various orientations (Fig. 1g and Supplementary video. S2).

The whole robotic structure includes a 4-DoF origami parallel mechanism, a metal base, four motors, and four sets of transmission linkages (Fig. 1a). The parallel mechanism and the motors are fixed at the metal base, and four sets of transmission linkages are connected between the limbs and the motors.

We select a 4-DoF 3T1R (three translations plus one rotation) parallel mechanism[26,27] and minimize it to the millimeter scale through the SCM method. The origami transmission mechanism is fabricated following the “split and splice” strategy. Each limb of the transmission mechanism contains a parallel-four-bars linkage, which is folded and fixed by two pieces of alumina ceramics. The moving platform is formed by two pieces of alumina ceramics with variable interfaces for attaching different end-effectors (Fig. 1c). The origami parallel mechanism weighs 2.48 g. It can fold up to a minimum size of 23.75 mm × 23.75 mm × 32.1 mm (Supplementary material Note. S1).

Each limb has an actuation joint, which is the joint closest to the fixed platform. The link of the origami transmission mechanism and the transmission linkage together form a parallelogram. Thus, for each limb, the angle of the actuation joint is equal to the angle of the corresponding motor (Fig. 1d).

The origin of the fixed platform and the moving platform are set as G and P, respectively. The position of the coordinate P with respect to coordinate G is defined as the position of the moving platform (Fig. 1a). The initial configuration of the robot is defined as the position of the moving platform at (x_m,y_m,z_m,α_m) = (0 mm, 0 mm, 24 mm, 45 [deg]). At this initial configuration, the input combination is $(\theta_1,\theta_2,\theta_3,\theta_4)$ = (− 4.23, − 4.23, − 4.23, − 4.23) [deg]. Considering the mechanical interference of the 4-DoF origami transmission mechanism, the input limitation of the actuation joint is set as [− 41, 23] [deg].

Workspace measurements and verification

Workspace measurement is categorized into constant-orientation workspace and total-orientation workspace. Constant-orientation workspace is defined as the maximum space the moving platform can reach while maintaining its orientation. In this work, it is obtained when α_m = 45 [deg]. The total orientation workspace is defined as the maximum space that the moving platform can reach while the rotation range is large enough to cover the selected angles. In this work, the orientation ranges [15, 75] [deg] and the workspace is obtained as the intersection shape of two constant-orientation workspaces with α_m = 15 [deg] and 75 [deg], the analysis of this workspace is detailed in Supplementary material Note. S5.

The measured outlines of the constant-orientation workspace and total orientation workspace are compared with the theoretical calculation result (Fig. 2). The measurements process are performed in Supplementary video. S3.

The experimental data indicates that the outlines of the workspace coincide very well with the kinematic model except for slight distortion at sharp corners in the constant-orientation workspace. The sources of these errors are discussed in the Supplementary material Note. S7. The volume of the workspace can be measured from the kinematic model. The volume of the constant-orientation workspace and the total orientation workspace are measured as 756 mm^3 and 362 mm^3, respectively.

Precision measurements

The precision characterization of the Micro-X4 is separated into two terms: positioning repeatability and orientation repeatability. For positioning repeatability, we select nine representative points

(Supplementary materials Note. S8) among the constant-orientation workspace of the robot with 10 times repeated visits and 100 recording points per visit (Supplementary video. S4 and Supplementary materials Note. S9). The attained positions along each axis are recorded separately. The uniaxial repeatability is calculated based on the standard deviation of the attained position with respect to the average position. The results are:$RP_x = 270$ nm, $RP_y = 180$ nm, $RP_z = 120$ nm. The overall positioning repeatability is calculated as $RP = (RP_x^2 + RP_y^2 + RP_z^2)^{\frac{1}{2}}$, which is ~346 nm. The orientation repeatability is measured at the initial configuration. We maintain the position of the robot at this point while rotating the moving platform back and forward between 0 [deg] and 90 [deg] for 5 cycles with totally 1000 recording points. The orientation repeatability is calculated as the standard derivation of the experiment data, which is ~0.17 mrad.

Supplementary video S5 demonstrates the large workspace and high precision advantages of the Micro-X4. The micromanipulator can point the vertices and midpoints of two squares of different scales, 5 mm and 10 μm (Fig. 2c). It proves that the Micro-X4 can perform large workspace while maintaining high precision.

Stiffness and force measurements

One of the most attractive properties of the Micro-X4 is its high stiffness compared with other origami robots. These advantages enable the micromanipulator to meet the requirements of contact operations such as detection, puncturing, cutting, and injection while maintaining positioning precision. The statistical stiffness of the robot is measured by maintaining the motors and applying forces on the moving platform. We measure the compressive and torsional stiffness with different robot configurations. The tested points are the same as the precision test, the block force along the X, Y, and Z axis and the block torque along the Z' axis are recorded in Fig. 3a–d and Supplementary materials Notes. S10. The measurement processes are recorded in Supplementary video S6.

The block force and torque are selected as the deflection of the moving platform at 50 μm or 0.5 [deg]. For translational motion, the average block forces are 0.1369 N, 0.1762 N, and 1.173 N along the X, Y, and Z-axis, respectively. The average block torque is 0.757 N × mm. The compressive and torsional stiffness are calculated as the secant stiffness: $K^T = \frac{\text{Block force@50}\mu m}{50\mu m}$ or $K^R = \frac{\text{Block torque@0.5[deg]}}{0.5[\text{deg}]}$. The corresponding stiffness are $K_x^T = 2738$ N/m, $K_y^T = 3524$ N/m, $K_z^T = 23460$ N/m and $K_z^R = 1.514$ N × mm/[deg], respectively. The overall stiffness for the whole mechanism is reported as the minimum stiffness along the X-axis, which is 2738 N/m. The high compressive and torsional stiffness pave the way for further tasks with contact operations.

Trajectory and bandwidth measurements

In the trajectory test, four shapes are selected to demonstrate the executing capability of the Micro-X4: "Z" shape, star, square, and circle. We test the trajectories with four scales: 50, 500, 2000, and 4000 μm.

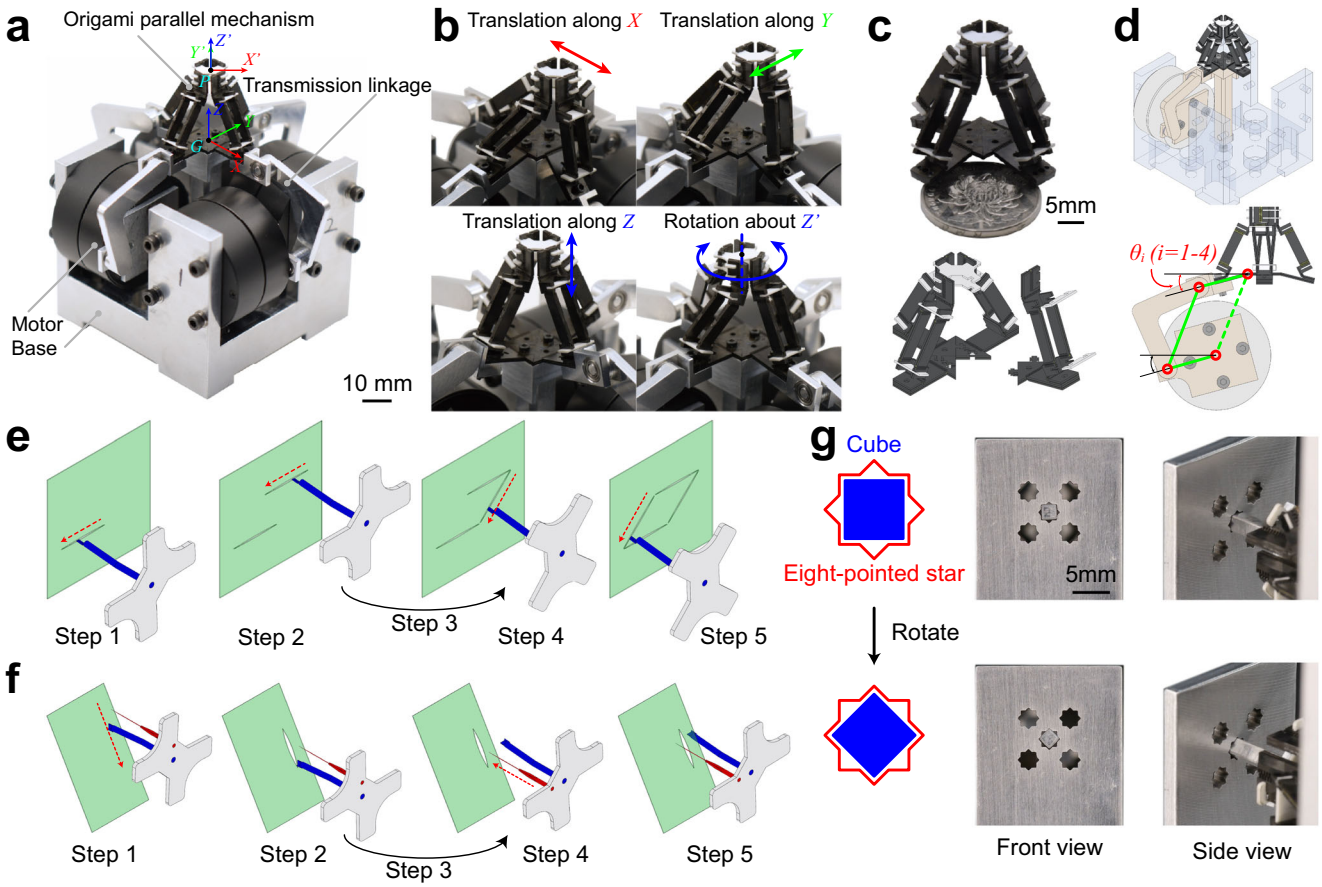

Fig. 1 | Robot design. a Image of the Micro-X4. The origins of the fixed platform and the moving platform are set as G and P, respectively. **b** Demonstrations of the four DoFs. **c** Image of origami parallel mechanism and the exploded illustration of the Computer-Aided Design (CAD) model. A coin is included for scale. **d** Perspective CAD model and the transmission linkage. The link of the origami parallel mechanism, the transmission linkage, and the arm of the motor together form a parallelogram. The input angle of the origami parallel mechanism is equal to the angle of the motor. **e** Pattern cutting with a knife end-effector. Step 1: cut the bottom line. Step 2: cut the top line. Step 3: rotate the orientation of the blade. Step 4: cut the right line. Step 5: cut the left line to close the pattern. **f** Cell surgery with two end-effectors: a knife and a needle. Step 1-2: cut an opening with the knife. Step 3: rotate to switch to the needle. Step 4-5: insert the needle through the opening. **g** Utilizing the rotational DoF to insert the cube into eight-pointed star holes with different orientations.

The frequencies are selected as 0.05, 0.1, 0.5, 1, and 2 Hz for scales under 500 µm. For trajectories at 2000 µm and 4000 µm, the test frequency is selected as 0.05 Hz and 0.1 Hz to avoid distortion. Selected trajectories are performed in Fig. 3e–h and Supplementary video S7. We also test the maximum speed of Micro-X4 as ~124 mm/s by driving the moving platform back and forward along a 12.4 mm line at 5 Hz.

We further calculate the trajectory repeatability to evaluate the performance of the execution and to analyze the relationship between the trajectory repeatability and the execution conditions. The metrics are calculated across five cycles and demonstrated in Fig. 3i and j. For all tests at 50 µm, the trajectories show no significant differences, all repeatability are smaller than 2 µm. At the fixed frequency of 0.05 Hz, the repeatability gradually deteriorates as the scale increases but remains within 6 µm. Overall, the Micro-X4 exhibits high trajectory repeatability.

Micromanipulation demonstrations

To demonstrate the micromanipulation capabilities of the Micro-X4, we present four examples highlighting its performance. Attributed to characteristics such as large workspace, high stiffness, high precision, and dexterity, the Micro-X4 is capable of covering micromanipulation tasks at multiple scales[28] from large to small: tissue - cellular - subcellular. The sensing capability of the Micro-X4 is further demonstrated through the achievement of contact force measurement and precise cell contact operation.

Pattern cutting. Soft tissue manipulation[2] is the fundamental of neurosurgery[29,30], eye surgery[31,32], and facial transplantation[33,34]. These microsurgeries required the accuracy and dexterity of tissue manipulations such as cutting, peeling, transplantation, and insertion. Among these, cutting specific patterns on tissue is one of the most important procedures. Here we demonstrate the Micro-X4 with cutting patterns on the onion slice (Supplementary video S8). In this demonstration, a knife is fixed in the middle of the moving platform (Fig. 4a). We show that the Micro-X4 can cut diamond patterns at different scales (Fig. 4b and c). For other shapes, we can separate them into multiple diamond elements and then cut the outlines of the elements to fit the shape (Fig. 4d). Here, we perform two patterns: a 5 mm circle and a 5 mm square (Fig. 4e and f). It is shown that the Micro-X4 is capable of cutting patterns with different scales and shapes, which is an important application in microsurgery.

Cell locating and puncturing. Cell injection is one of the most important topics in cell manipulation research, which has wide application in fertilization[3] and drug delivery[35]. Robotic microinjection[36,37] is gaining popularity over manual injection for its accuracy and efficiency. The rapid and precise locating of the injection target is a crucial factor in promoting injection efficiency. Here we demonstrate the robot's capability to locate and puncture cells by a needle end-effector (Fig. 4g and Supplementary video S9). We demonstrate the Micro-X4 aligning the needle tip to a selected cell nucleus within a stained onion slice (Fig. 4h). The Micro-X4 can also puncture the onion cells using the needle (Fig. 4i). This experiment proves the potential of the Micro-X4 to serve as a platform for high-throughput microinjection.

Cell cutting and inserting. Cell surgery[38] provides a strategy for understanding the fundamentals of genes and diseases, which requires subcellular manipulation[39]. Different cell surgeries generally apply different end-effectors to meet different tasks such as cell holding[3], biopsy[9], cutting[40] and nuclear transfer[41]. With the evolvement of cell surgery, surgical procedures are becoming more intricate, demanding a wider array of tools and end-effectors. Taking yeast cell microinjection as an example, rigid cell walls are difficult to penetrate, which is required to break the cell walls before injection. To conquer this difficulty, mechanical[42] and electroporation[43] methods are introduced in previous researches, and those methods make the entire surgical process more complex. To simulate the process of microinjection with rigid cell walls, we execute a simulation on a cabbage cell (Supplementary video S10). The Micro-X4 is equipped with two end-effectors, a blade and a needle (Fig. 4j). The micromanipulator can cut a line on the cell with the blade to create an opening (Fig. 4k), and then rotate the moving platform to switch the end-effector to the needle. Finally, the manipulator extends the needle into the interior of the cell along this opening (Fig. 4l). It is shown that the Micro-X4 is capable of equipping multiple end-effectors and achieving end-effector switching, which proves that Micro-X4 is a possible tool for complex cell surgery and sub-cellular micromanipulation tasks.

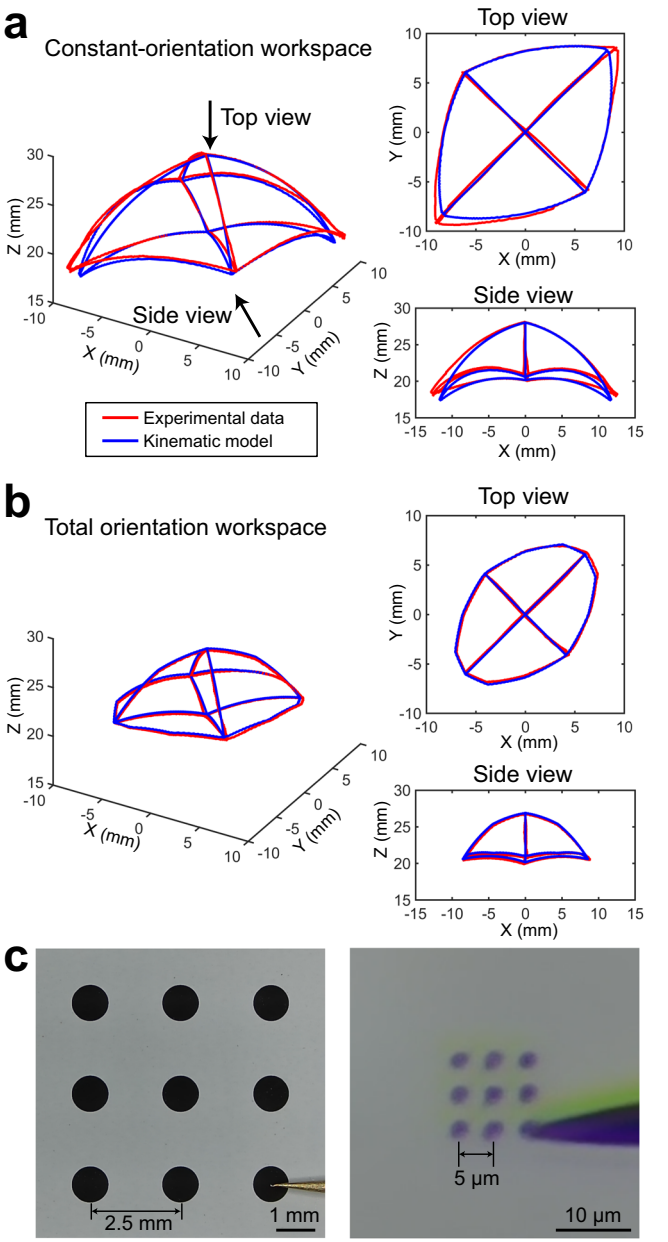

Fig. 2 | Workspace and precision measurements. a, **b** Constant-orientation workspace and total orientation workspace. Comparisons between the experimental data and the kinematic model with different views. **c** Locating points at different scales (left 5 mm, right 10 μm). Source data of (**a** and **b**) are provided as a Source Data file.

https://doi.org/10.1038/s41467-025-57815-5

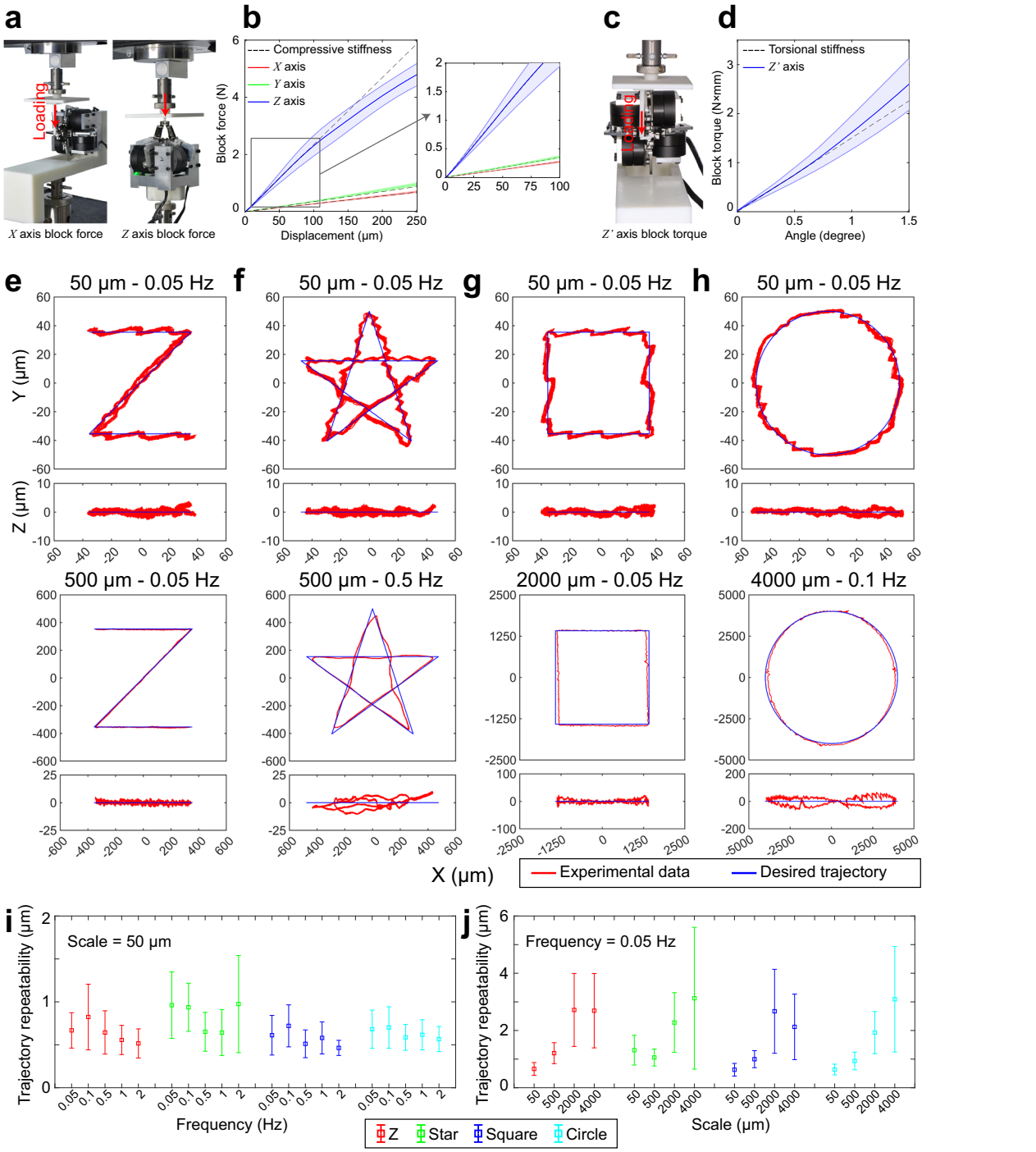

Fig. 3 | Stiffness and trajectory measurements. a Experimental setup for block force measurements. **b** Block force and compressive stiffness with *X*, *Y*, and *Z*-axis. The shaded error bar represents the standard deviation. **c** Experimental setup for block torque measurements. **d** Block torque and torsional stiffness about *Z*′ axis. The shaded error bar represents the standard deviation. **e** Z trajectories. **f** Star trajectories. **g** Square trajectories. **h** Circle trajectories. **i** Repeatability of different trajectories at 50 μm and frequency ranges [0.05, 2] Hz. The error bar represents the standard deviation. **j** Repeatability of different trajectories at 0.05 Hz and scale ranges [50, 4000] μm. The error bar represents the standard deviation. Source data are provided as a Source Data file.

Cell touching and puncturing. The Micro-X4 is equipped with a thin film pressure sensor between the end-effector and the moving platform, demonstrating the feasibility of integrating sensing capabilities within micromanipulation in an origami micromanipulator. The sensor enables the robot to acquire contact force during operations. Based on this, we execute a cell touching and puncturing experiment. The Micro-X4 is equipped with the sensor and a needle (Fig. 4m). The robot alternately performs the 'touching - puncturing - touching - puncturing - touching - puncturing' sequence along a series of six onion cells (Fig. 4o). 'Touching' refers to the operation where the needle tip contacts the cell, causing it to deform noticeably. 'Puncturing' refers to the operation of piercing the cell. This demonstrates that precise contact operations can be achieved with the origami micromanipulator by measuring the contact force (Fig. 4n). This experiment is recorded in Supplementary video S11. The devices and control algorithm can be found in Methods section 'Contact operation force control'.

https://doi.org/10.1038/s41467-025-57815-5

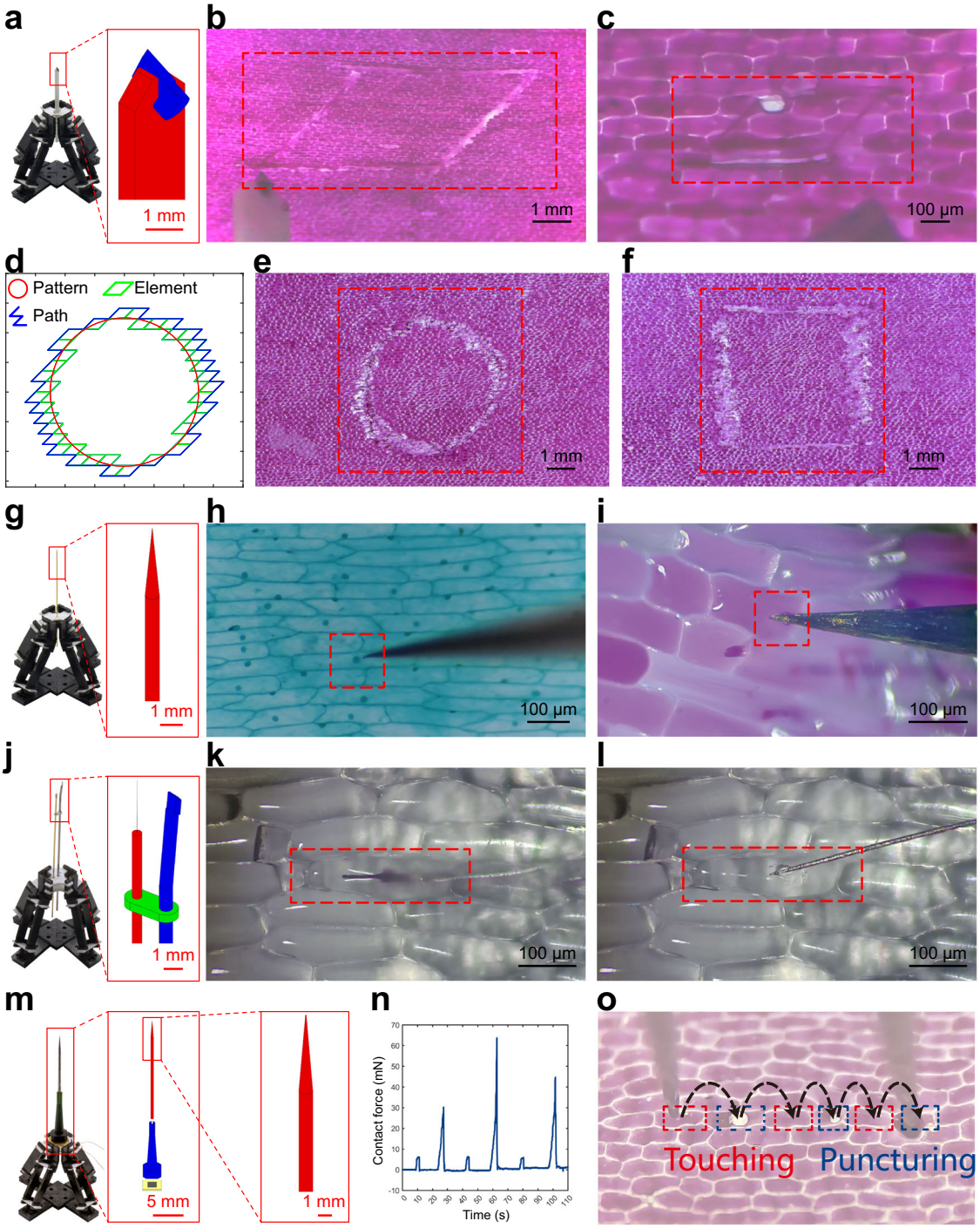

Fig. 4 | Micromanipulation demonstrations. a Image of the Micro-X4 with a blade end-effector for pattern cutting. **b**, **c** Cutting diamond shape patterns at 5 mm (**b**) and 500 μm (**c**). **d** Illustration of trajectory planning for circle pattern. **e**, **f** Cutting circle (**e**) and square (**f**) patterns at 5 mm. **g** Image of the Micro-X4 with a needle end-effector for cell locating and puncturing. **h** Locating the cell nuclei of a stained onion slice. **i** Puncturing the onion cell. **j** Image of the Micro-X4 with two end-effectors, a blade, and a needle. **k** Cutting an opening on the cabbage cell with the blade end-effector. **l** Inserting through the opening with the needle end-effector. **m** Image of the Micro-X4 with a needle end-effector and a pressure sensor for contact force measurement. **n** Contact force during the operation sequence. **o** Touching and puncturing a series of cells through contact force control. Source data of (**n**) are provided as a Source Data file.

Discussion

To summarize, the micromanipulation demonstrations prove that the Micro-X4 can execute multiple tasks from the tissue scale to the sub-cellular scale. By integrating the origami design, including flexible hinges and flat-foldability, we can rapidly fabricate complex closed-loop parallel mechanisms, further enhancing the assembly and execution precision of the robot. Compared to the state-of-the-art origami micromanipulators, the Micro-X4 offers large workspace (756 mm^3), high precision (346 nm), and high stiffness (2738 N/m) to cover the requirements of the practical application. We conduct a

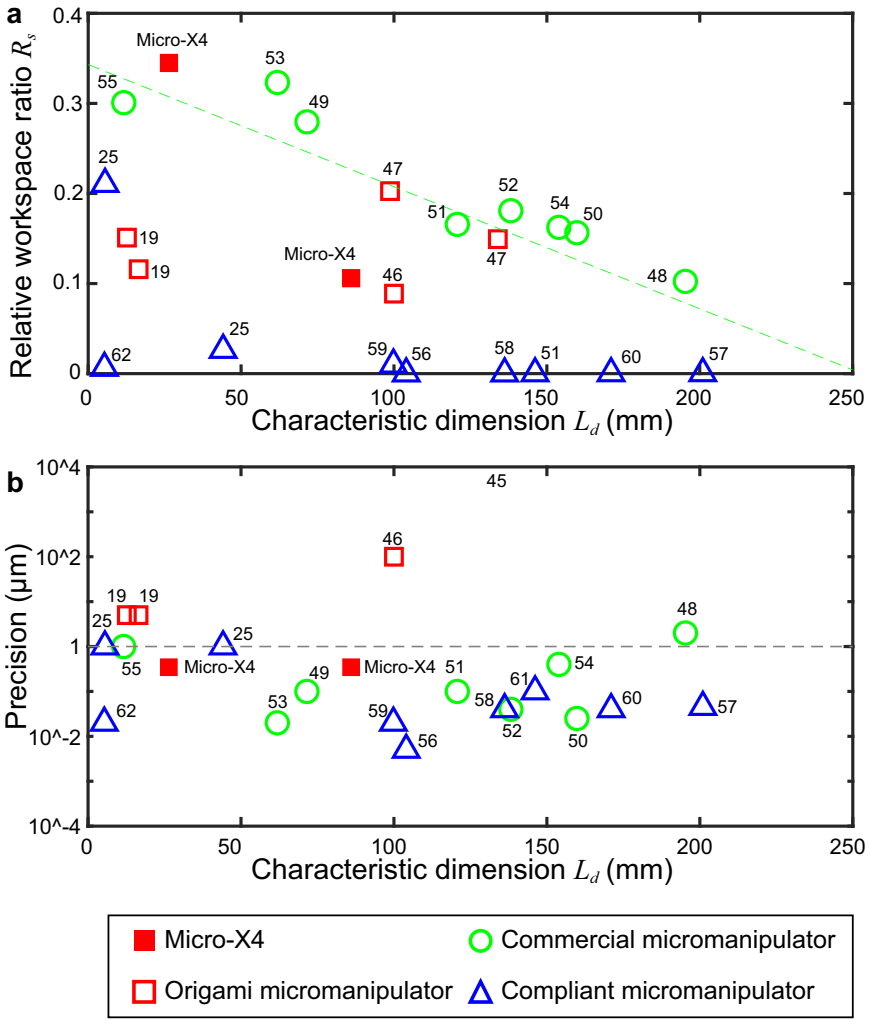

Fig. 5 | Performance comparison of Micro-X4 with other micromanipulation platforms. The origami transmission mechanism of the Micro-X4 has one of the highest relative workspace ratio R_S (**a**). Micro-X4 is also the first origami micromanipulator to achieve sub-micron precision (**b**). For duplicated items, one refers to the parallel mechanism with a small characteristic dimension, the other refers to the entire set of equipment with large characteristic dimension.

comparison between the Micro-X4 and several other micromanipulation platforms to demonstrate the advantages of our work in compact size, large relative workspace, and high precision (Methods section 'Performance comparison' and Fig. 5). In addition, the rotational DoF endows the Micro-X4 with dexterity in complex tasks such as cutting patterns or switching end-effectors. This study is expected to provide new strategies for robotics and origami research, specifically in the construction of origami micromanipulators, and to offer a new tool for fields such as biology, medicine, and micro-automation.

From the aspects of fabrication, the Micro-X4 is one of the most complex structures in the field of origami micromanipulators for its four limbs and total 48 joints. To conquer this fabrication challenge, we propose the "split and splice" method, which can be further applied in other complex origami structures. From the aspects of actuation and control, the analytical kinematic model for origami structures can be referred to as the modeling of other origami structures.

Although the proposed Micro-X4 exhibits high precision for its repeatability, the absolute accuracy of most origami micromanipulators, including this robot, is not high enough. From the perspective of the origami mechanism, the reasons include low material modulus and the influence of the torque generated by the soft joint on the mechanism configuration during large rotating angles. We plan to develop an error evaluation model to analyze the impact of the aforementioned factors on the configuration and end pose of the robot. The model can guide the material selection, geometric design, and driving method of the origami micromanipulator. We expect to optimize the absolute accuracy to within 10 μm.

Further research will focus on the integration of the Micro-X4 with other devices to expand the manipulation capability(Fig. 6). In microsurgery, the Micro-X4 can be connected to the end of a large series manipulator. In this case, the series manipulator plays the role of the platform to a target location and orientation, while the Micro-X4 works as the end-effector for high-precision manipulation. Several Micro-X4 can be integrated to construct a multiple robots platform for complex manipulation tasks or to promote manipulation efficacy. In cell manipulation and microassembly, functional end-effectors can be developed to perform more complex contact operations such as grasping and adhesion.

Methods

The "split and splice" method

Microstructures containing close-loops, such as micro-parallel mechanisms are generally hard to fabricate with traditional methods. The SCM method provides a powerful tool for fabricating microstructures with massive joints. For a micro parallel mechanism with the SCM method, a generic method for designing the fabrication process

https://doi.org/10.1038/s41467-025-57815-5

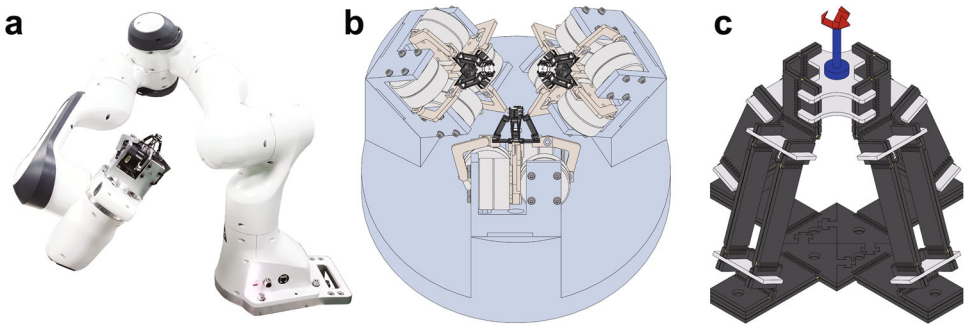

Fig. 6 | Further applications of Micro-X4. a Integrate with a series manipulator as an end-effector. **b** Construct a multi-robot platform for complex manipulation tasks. **c** Equipped with functional end-effectors (a micro gripper).

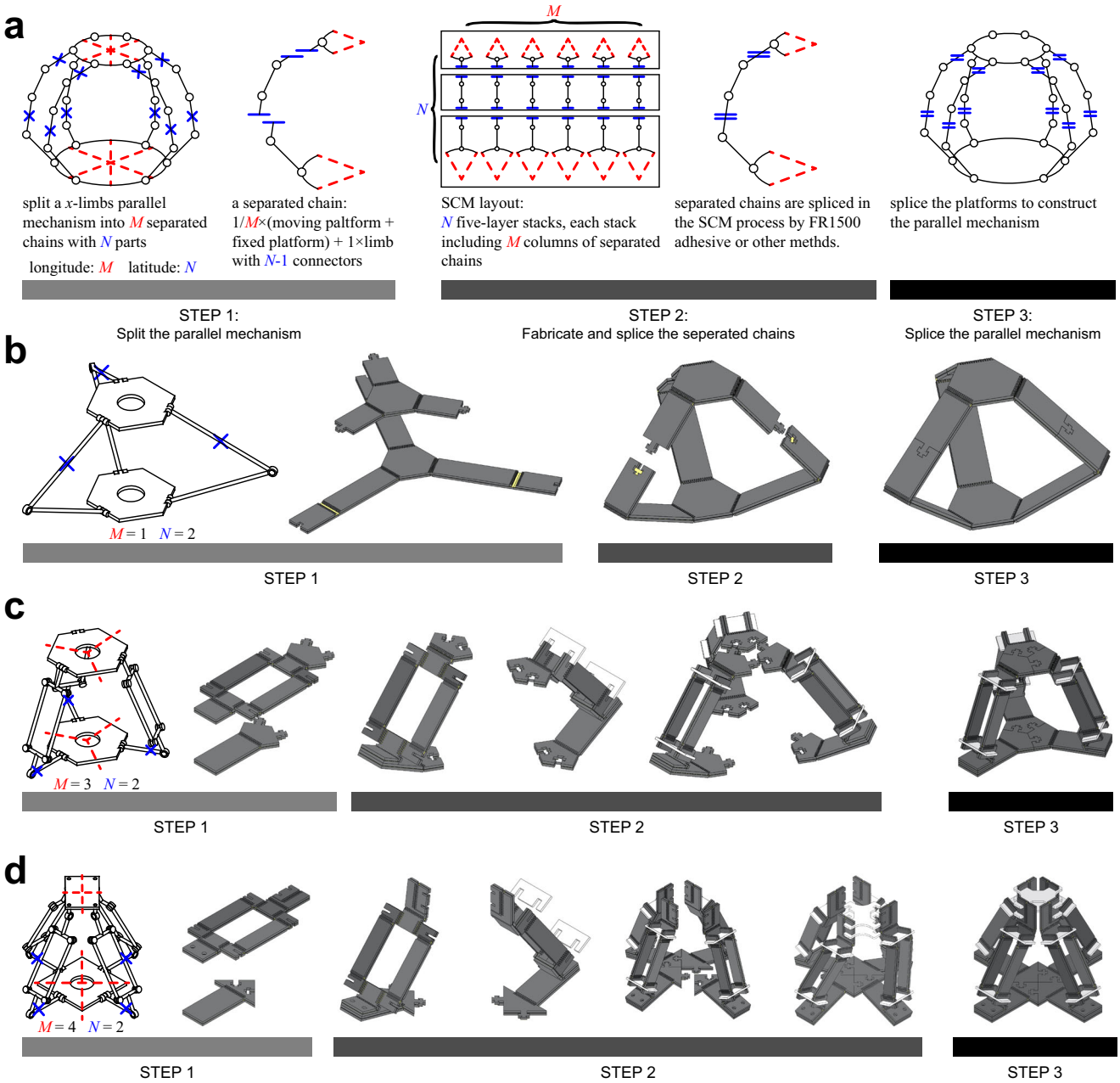

Fig. 7 | The "split and splice" method for Smart Composite Microstructure (SCM) process. a The demonstration of the method. **b**–**d** The examples on Sarrus mechanism (**b**), Delta mechanism (**c**) and origami transmission mechanism of the Micro-X4 (this work) (**d**).

can greatly reduce the difficulties and complexities of the manufacturing. Here we present the "split and splice" method to expand the scope of the SCM method to the micro close-loop structures and micro parallel mechanisms. The idea can be demonstrated in three steps (Fig. 7a).

The first step is to split the x-limb parallel mechanisms twice. The first time, the mechanism is separated into M separated chains, this splitment is under the longitude direction. The second time, each separated chain is splited into N parts. Thus, the parallel mechanism is totally splited into $M \times N$ parts. The second step is to fabricate the separated chains by the SCM method. Since the close-loops are broken in the first step, the planarized process is easy to achieve here. The parts are connected into separated chains by adhesion and key-keyhole[22,44] connection. Finally, the separated chains are connected into a complete closed-loop parallel mechanism.

The selection of the splitment need to follow the rules:

- In the longitude direction, for an x-limbs parallel mechanism, the parameter M is generally selected as $M \le x$ to avoid redundant platform fragments.
- In the latitude direction, for a limb with y joints, the parameter N is generally selected as $N \le y$ to avoid redundant limb fragments.

The X4 parallel mechanism is a 4-limb mechanism, and each limb contains a parallel-four-bar linkage. In this work, the "split and splice" is successfully applied to fabricate a millimeter scale Micro-X4 mechanism through the SCM method. We also provide two other demos, the Sarrus mechanism and Delta mechanism, via the "split and splice" method (Fig. 7b–d). The complete SCM process of the Micro-X4 is demonstrated in Supplementary Material Note. S1. The manufacturing error of the origami transmission mechanism is analyzed in Supplementary Material Note. S2.

Kinematic model

The kinematic model of the Micro-X4 bears a resemblance to the conventional X4 structure's kinematic model, albeit with a few significant modifications. Notably, a primary difference between the origami structure and the traditional kinematic model is observed in the geometry of the parallelogram linkages within each limb. The presence of parallelogram linkages within the limb is a standard design feature in parallel mechanisms with translational DoFs. Typically, these linkages are arranged in series between two revolute joints (Fig. 8a). In conventional industrial robots, this limb kinematics are often achieved by utilizing four universal joints or spherical joints with specific constraints (Fig. 8b). The coinciding axes of these joints facilitate ease in kinematic models.

While in the SCM structure, we split the limb to make it available for the planarized fabrication process. We prefer to fabricate these linkages by individually revolute joints, which leads to a bias between the revolute joints and the parallelogram linkage (Fig. 8c). The impact of this deviation has been discussed in milliDelta robot[19], where it slightly affects the workspace's shape.

In the kinematic model, disregarding the bias generated by the characteristics of the origami structure won't affect the repeatability performance, but it will affect the accuracy of the motion. For instance, executing trajectories may result in distortion (Fig. 8d). To address this issue and promote execution accuracy, we propose an inverse kinematic model that accounts for this bias. A comprehensive derivation is detailed in Supplementary Material Note. S4.

Actuation and control method

The control architecture of the Micro-X4 is illustrated in Fig. 9. The Micro-X4 is actuated by four motors equipped with encoders (DM-R-3505, HAITAI). The target position for these motors is determined using the inverse kinematic model with the desired destination. The motor's position is sampled by the encoder, enabling the computation of the motor's velocity based on its position. The target velocity is set at 60 [deg]/s, and the current is limited to 1.02 A. All these data are gathered by the field-oriented control driver. Three Proportional-Integral-Differential (PID) controllers are implemented within the field-oriented control driver to compute the driving signal according to the target position, velocity, and current. The calibration process of the PID controller is demonstrated in Supplementary Material Note. S6. Subsequently, this driving signal is transmitted to the motor, enabling the origami transmission mechanism to achieve the desired destination.

Contact operation force control

The thin film pressure sensor PXS-S6ST-50K (GuanZhou PuHui Technology Co.Ltd) is fixed between the moving platform and the needle to measure the normal force along the needle. During the cell contact operation process, we primarily focus on three values: the current value of the sensor F_t, the minimum value recorded in this operation F_{min}, and the maximum value F_{max}.

For the cell touching operation, we set an upper limit for the contact force F^U, when F_t achieve or above the upper limit, the needle will hold on for a while and retract. The algorithm is shown in Algorithm 1. During the cell puncturing process, precise control of the needle is critical to ensure that cells are punctured rather than cut through. With force measurement, we are able to monitor the change in the contact force. A rapid decrease implies that the cell has already been punctured. Based on this judgment, we set the puncture force threshold $R = 0.18$, meaning that when F_t is below 82% of the maximum puncturing force ($F_{max} - F_{min}$), the needle tip will retract. This ensures that only the cell wall is punctured without penetrating the entire cell. The process is demonstrated in Algorithm 2.

Algorithm 1. Cell touching

while Touching command starts **do**
  if $F_t < F^U$ **then** (*Contact force not achieve the upper limit*)
    Needle tip keeps going down
  else
    Needle tip stays in the current position for a while
    Needle tip lifts
    break
  end if
end while

Algorithm 2. Cell puncturing

while Puncturing command starts **do**
  if $F_t < F^U$ **then** (*Before puncturing, ensure contact with the cell*)
    Needle tip keeps going down
  else
    if $(F_{max} - F_t) \ge R(F_{max} - F_{min})$ **then** (*A rapid decrease in contact force implies that the cell has been punctured*)
      Needle tip lifts
      break
    else
      Needle tip keeps going down
    end if
  end if
end while

Performance comparison

The characterization results of the Micro-X4 are compared with several other micromanipulation devices. To standardize the performances of different platforms, we utilize several metrics. The characteristic

https://doi.org/10.1038/s41467-025-57815-5

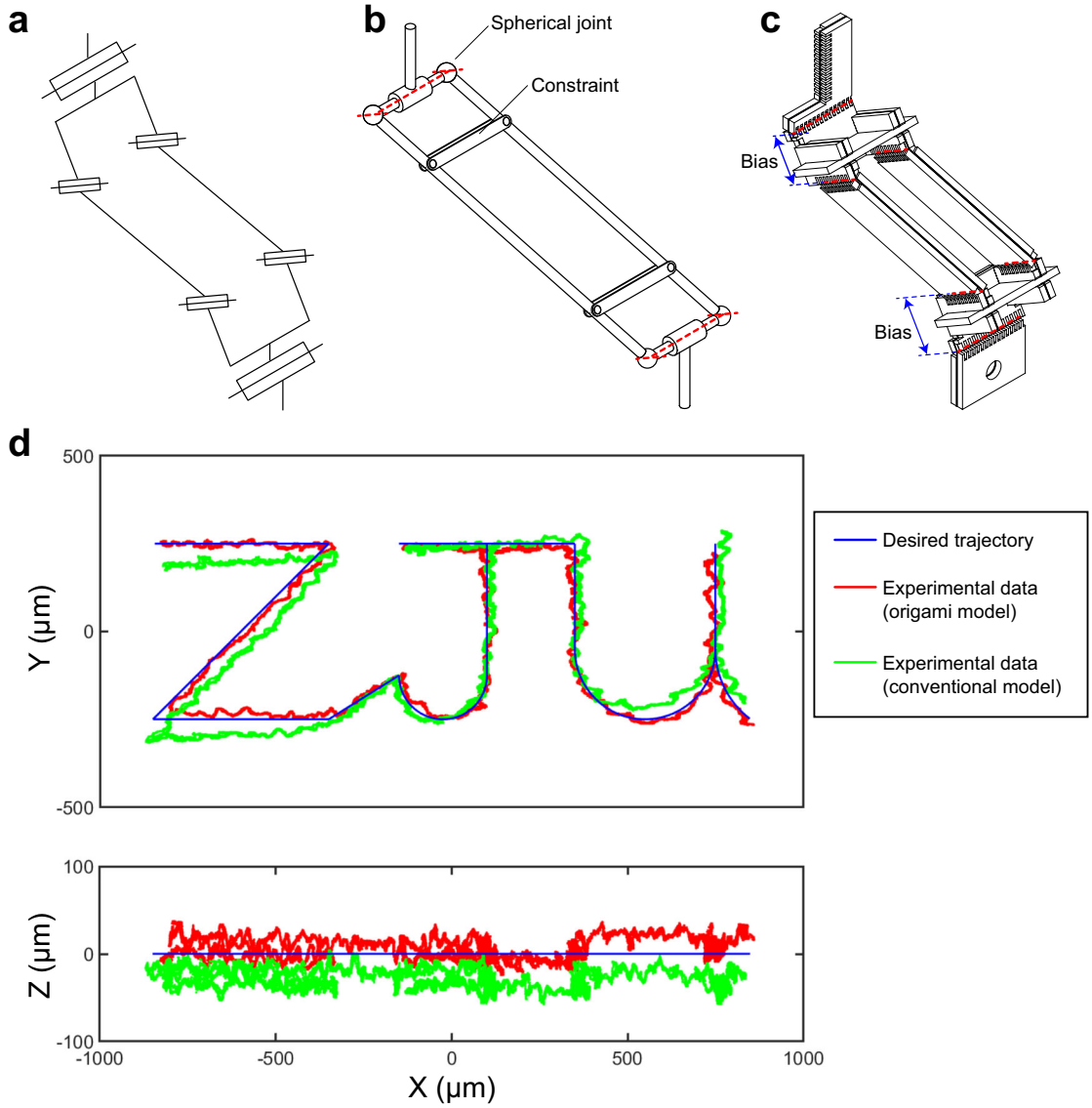

Fig. 8 | Parallelogram linkages in mechanical structure and origami structure. **a** Theoretical model of a limb contains parallelogram linkage. The linkage is in series between two revolute joints. **b** Conventional mechanical design of the limb. Revolute joints and the parallelogram linkage are achieved by four spherical joints with extra constraint links. The axes of the revolute joints and the axes of the joints in parallelogram linkage are coplanar. **c** Origami design of the limb. Due to the limitations of the SCM process, bias exists between the revolute joint axis and the parallelogram linkage. **d** Trajectories of the "ZJU". The size of the desired trajectory is 1700 μm × 500 μm. The trajectory executed followed the conventional model is different from the origami model. In the XY plane, there is an anticlockwise rotation of ~4.3 [deg] with respect to the origami model. In the XZ plane, the trajectory of the convention model is ~33 μm lower than the origami model. Source data of (**d**) are provided as a Source Data file.

dimension L_d of the platform is defined as:$L_d = \text{Volume}^{\frac{1}{3}}$ mm. The dimensionless relative workspace ratio R_s[45] is defined as: $R_s = \frac{\text{Workspace}^{\frac{1}{3}}}{L_d}$. We select three types of micromanipulation platforms: origami micromanipulators[19,46,47], commercial micromanipulators[48–55], and compliant micromanipulators[25,56–62].

The actuators of certain platforms occupy a relatively large proportion of the mechanism. For example. the Micro-X4 holds potential for further miniaturization by replacing smaller motors (Supplementary material Note. S12.). Therefore, the main bottleneck in the further miniaturization of such platforms is the actuators rather than the mechanism, as indicated by references[19,25,47] and Micro-X4.

For these devices, we have calculated the volume and other corresponding indicators separately for both the parallel mechanism and the entire set of equipment. Regarding precision metrics, some studies have reported the repeatability of the devices, while others have used resolution or have converted it.

Origami micromanipulators exhibit a smaller volume ($L_d \leq 150$ mm), an average R_s (with values ranging from 0.1 to 0.2), and a precision worse than 1 μm. Commercial micromanipulators generally follow the rule that a larger L_d corresponded to a smaller relative workspace R_s. These devices typically maintain high precision and mostly achieve sub-micron. Regarding compliant micromanipulators, most of them exhibited a small relative workspace ($R_s \leq 0.1$), but all have precision below one micron. In comparison to these platforms, the parallel mechanism of the Micro-X4 exhibits one of the highest R_s values. Moreover, the Micro-X4 stands as the first origami micromanipulator to achieve sub-micron precision. Among all platforms with $L_d \leq 30$ mm, the parallel mechanism of the Micro-X4 shows one of

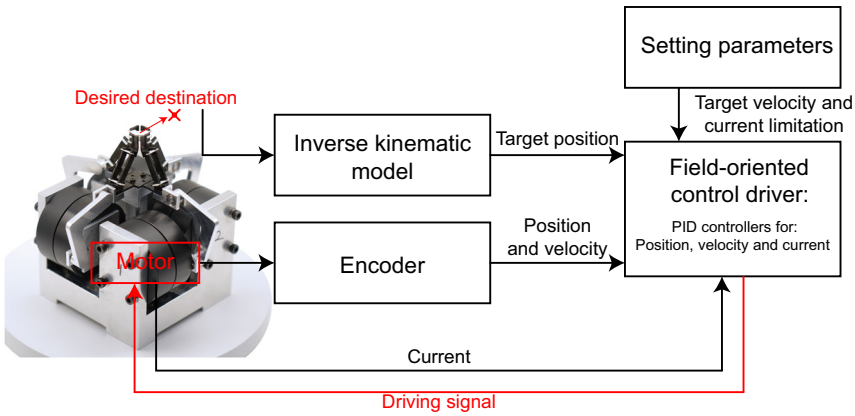

Fig. 9 | Control architecture of the Micro-X4. The target motor position is determined using the inverse kinematic model with the desired destination. The motor's position is sampled by the encoder and subsequently transmitted to the Field-Oriented Control driver. The motor's velocity is calculated from the encoder position. The target velocity is manually set. The motor's current is sampled by the Field-Oriented Control driver, and its limitation is manually set. The calculated driving signal is then sent to the motor.

Table 1 | Relevant parameters for a selection of micromanipulation platforms

	Name	Size (mm)	Characteristic dimension L_d (mm)	Workspace (mm^3)	Relative workspace ratio R_s	Precision (μm)
Origami	milliDelta[19]	15 × 15 × 9.05*	12.7	7.01	0.151	5
		15 × 15 × 20	16.5	–	0.116	–
	Correa et al.[46]	100 × 100 × 100*	100	700*	0.089	100
	Kalafat et al.[47]	D175 × H40*	98.7	8000	0.202	\
		D280 ×;H70*	162.7		0.123	
	Micro-X4 (This work)	24 × 24 × 32	26.4	756.2	0.345	0.346
		85 × 85 × 88	86		0.106	–
Commercial	MX7600[48]	208 × 173 × 206	195.0	8000	0.102	2
	uMP-3|4[49]	39 × 93 × 101	71.5	8000	0.280	0.1
	SM 3.25[50]	178 × 126 × 182	159.8	15625	0.156	0.025*
	PatchStar Micromanipulator[51]	110 × 78 × 205	120.71	8000	0.165	0.1*
	MP-285[52]	110 × 150 × 160	138.2	15625	0.181	0.04*
	InjectMan® 4[53]	129 × 51 × 36	61.9	8000	0.323	0.02*
	M-VP-25XA-XYZL[54]	126 × 144 × 201	153.9	15625	0.162	0.4
	MS15 xyz-mounted[55]	15 × 7 × 15	11.6	42.875	0.301	1
Compliant	MiGribot[25]	19 × 22 × 0.4	10.68	1.56*	0.211	1
		38.5 × 38.5 × 58.0*	44.1	–	0.026	–
	Wu et al.[56]	150 × 150 × 50	104	5.4×10^{-7}	7.83×10^{-5}	0.005*
	Zhang et al.[57]	D264 × H148.4	201	3.84×10^{-4}	3.61×10^{-4}	0.045
	Cai et al.[58]	D150 × H143	136.2	1.14×10^{-6}	7.66×10^{-5}	0.04*
	Ahn et al.[59]	180 × 180 × 30.7	99.8	0.972	0.010	0.02*
	Varadarajan et al.[60]	250 × 250 × 80	171	1.28×10^{-4}	2.94×10^{-4}	0.04*
	Furutani et al.[61]	170 × 170 × 108	146.1	4×10^{-5}	2.34×10^{-4}	0.1*
	Zhang et al.[62]	10 × 10 × 1.5	5.31	3.78×10^{-5}	0.006	0.02

The data not directly reported in the literature have all been calculated and estimated through the figures or converted from the reported data. These data are marked with an asterisk *. For milliDelta[19], Kalafat et al.[47], Micro-X4 and MiGribot[25], we duplicate these rows to compare performance of this items when considering or ignoring the dimensions of the actuators.

the best performances in terms of workspace and precision. The parameters of the platforms selected for comparison are listed in Table 1.

Data availability

All data generated or analyzed for this paper are included in the published article, its Methods, and Supplementary Information. Original videos and sensor data are available from the corresponding author on reasonable request. Source data are available at https://doi.org/10.5281/zenodo.14860767[63].

Code availability

Source codes are available at https://doi.org/10.5281/zenodo.14860767[63].

References

1. Zhang, Z., Wang, X., Liu, J., Dai, C. & Sun, Y. Robotic micromanipulation: Fundamentals and applications. *Annu. Rev. Control Robot. Auton. Syst.* **2**, 181–203 (2019).
2. Dogangil, G., Davies, B. L. & Rodriguez y Baena, F. A review of medical robotics for minimally invasive soft tissue surgery. *Proc. Inst. Mech. Eng. Part H. J. Eng. Med.* **224**, 653–679 (2010).
3. Sun, Y. & Nelson, B. J. Biological cell injection using an autonomous microrobotic system. *Int. J. Robot. Res.* **21**, 861–868 (2002).
4. Zhang, Y., Chen, B. K., Liu, X. & Sun, Y. Autonomous robotic pick-and-place of microobjects. *IEEE Trans. Robot.* **26**, 200–207 (2010).
5. Zhang, S. et al. Piezo robotic hand for motion manipulation from micro to macro. *Nat. Commun.* **14**, 500 (2023).
6. Banerjee, A. G. & Gupta, S. K. Research in automated planning and control for micromanipulation. *IEEE Trans. Autom. Sci. Eng.* **10**, 485–495 (2013).
7. Huang, H. et al. 3D Motion manipulation for micro- and nanomachines: Progress and future directions. *Adv. Mater.* **n/a**, 2305925 (2023).
8. Huang, H., Sun, D., Mills, J. K. & Cheng, S. H. Robotic cell injection system with position and force control: Toward automatic batch biomanipulation. *IEEE Trans. Robot.* **25**, 727–737 (2009).
9. Actis, P. et al. Compartmental genomics in living cells revealed by single-cell nanobiopsy. *ACS Nano* **8**, 546–553 (2014).
10. Tanikawa, T. & Arai, T. Development of a micro-manipulation system having a two-fingered micro-hand. *IEEE Trans. Robot. Autom.* **15**, 152–162 (1999).
11. Liu, X., Kim, K., Zhang, Y., Zhang, Y. & Sun, Y. Nanonewton force sensing and control in microrobotic cell manipulation. *Int. J. Robot. Res.* **28**, 1065–1076 (2009).
12. Aerts, J. T. et al. Patch clamp electrophysiology and capillary electrophoresis–mass spectrometry metabolomics for single cell characterization. *Anal. Chem.* **86**, 3203–3208 (2014).
13. Felton, S., Tolley, M., Demaine, E., Rus, D. & Wood, R. A method for building self-folding machines. *Science* **345**, 644–646 (2014).
14. Salerno, M., Zhang, K., Menciassi, A. & Dai, J. S. A novel 4-DOF origami grasper with an SMA-actuation system for minimally invasive surgery. *IEEE Trans. Robot.* **32**, 484–498 (2016).
15. Rus, D. & Tolley, M. T. Design, fabrication and control of origami robots. *Nat. Rev. Mater.* **3**, 101–112 (2018).
16. Zhang, Z. et al. Active mechanical haptics with high-fidelity perceptions for immersive virtual reality. *Nat. Mach. Intell.* **5**, 643–655 (2023).
17. Baisch, A. T., Ozcan, O., Goldberg, B., Ithier, D. & Wood, R. J. High speed locomotion for a quadrupedal microrobot. *Int. J. Robot. Res.* **33**, 1063–1082 (2014).
18. Chen, Y. et al. Controlled flight of a microrobot powered by soft artificial muscles. *Nature* **575**, 324–329 (2019).
19. McClintock, H., Temel, F. Z., Doshi, N., Koh, J.-s. & Wood, R. J. The milliDelta: A high-bandwidth, high-precision, millimeter-scale Delta robot. *Sci. Robot.* **3**, https://doi.org/10.1126/scirobotics.aar3018 (2018).
20. Kalafat, M. A., Sevinç, H. & Samankan, S. Design of a foldable origami-inspired 6-DoF Stewart mechanism. *J. Mech. Sci. Technol.* **38**, 1429–1438 (2024).
21. Mintchev, S., Salerno, M., Cherpillod, A., Scaduto, S. & Paik, J. A portable three-degrees-of-freedom force feedback origami robot for human–robot interactions. *Nat. Mach. Intell.* **1**, 584–593 (2019).
22. Suzuki, H. & Wood, R. J. Origami-inspired miniature manipulator for teleoperated microsurgery. *Nat. Mach. Intell.* **2**, 437–446 (2020).
23. Howell, L. L.*Compliant Mechanisms* (John Wiley & Sons, 2001).
24. Liu, Y. et al. Singularity analysis and solutions for the origami transmission mechanism of fast-moving untethered insect-scale robot. *IEEE Trans. Robot.* **40**, 777–796 (2024).
25. Leveziel, M., Haouas, W., Laurent, G. J., Gauthier, M. & Dahmouche, R. MiGriBot: A miniature parallel robot with integrated gripping for high-throughput micromanipulation. *Sci. Robot.* **7**, eabn4292 (2022).
26. Kim, S. M., Kim, W. & Yi, B.-J. Kinematic analysis and optimal design of a 3T1R type parallel mechanism. In *2009 IEEE International Conference on Robotics and Automation*, 2199–2204 (IEEE, Kobe, 2009).
27. Xie, F. & Liu, X.-J. Design and development of a high-speed and high-rotation robot with four identical arms and a single platform. *J. Mech. Robot.* **7**, https://doi.org/10.1115/1.4029440 (2015).
28. Nagle, M. P., Tam, G. S., Maltz, E., Hemminger, Z. & Wollman, R. Bridging scales: From cell biology to physiology using in situ single-cell technologies. *Cell Syst.* **12**, 388–400 (2021).
29. Karas, C. S. & Chiocca, E. A. Neurosurgical robotics: A review of brain and spine applications. *J. Robot. Surg.* **1**, 39–43 (2007).
30. Trybula, S. J., Oyon, D. E. & Wolinsky, J.-P. Robotic tissue manipulation and resection in spine surgery. *Neurosurg. Clin.* **31**, 121–129 (2020).
31. Haritoglou, C. et al. Long-term follow-up after macular hole surgery with internal limiting membrane peeling. *Am. J. Ophthalmol.* **134**, 661–666 (2002).
32. Baddon, A., Jones, M., Armitage, J., Warwick, R. & Kaye, S. A review of allograft ophthalmic tissue in eye surgery. *Cell and Tissue Banking* **11**, 29–38 (2010).
33. Schneeberger, S. et al. Achievements and challenges in composite tissue allotransplantation. *Transpl. Int.* **24**, 760–769 (2011).
34. Khalifian, S. et al. Facial transplantation: The first 9 years. *Lancet* **384**, 2153–2163 (2014).
35. Kaji, H., Nagai, N., Nishizawa, M. & Abe, T. Drug delivery devices for retinal diseases. *Adv. Drug Deliv. Rev.* **128**, 148–157 (2018).
36. Wang, W., Liu, X., Gelinas, D., Ciruna, B. & Sun, Y. A fully automated robotic system for microinjection of zebrafish embryos. *PLOS ONE* **2**, e862 (2007).
37. Han, Y. et al. The logic of single-cell projections from visual cortex. *Nature* **556**, 51–56 (2018).
38. Schubert, C. The deepest differences. *Nature* **480**, 133–137 (2011).
39. Shakoor, A., Gao, W., Zhao, L., Jiang, Z. & Sun, D. Advanced tools and methods for single-cell surgery. *Microsyst. Nanoeng.* **8**, 47 (2022).
40. Yang, R. et al. Cellular level robotic surgery: Nanodissection of intermediate filaments in live keratinocytes. *Nanomed. Nanotechnol. Biol. Med.* **11**, 137–145 (2015).
41. Yu, J., Zhao, Q., Cui, M., Sun, M. & Zhao, X. Robotic donor cell injection in Somatic Cell Nuclear Transfer (SCNT). In *Proceeding of the 11th World Congress on Intelligent Control and Automation*, 2821–2825 (IEEE, Shenyang, 2014).
42. Riveline, D. & Nurse, P. 'Injecting' yeast. *Nat. Methods* **6**, 513–514 (2009).
43. Tsuji, T., Yoshida, S., Yoshida, A. & Uchiyama, S. Cationic fluorescent polymeric thermometers with the ability to enter yeast and mammalian cells for practical intracellular temperature measurements. *Anal. Chem.* **85**, 9815–9823 (2013).
44. Liu, Y. et al. S2worm: A fast-moving untethered insect-scale robot with 2-DoF transmission mechanism. *IEEE Robot. Autom.Lett.* **7**, 6758–6765 (2022).
45. Richard, M. & Clavel, R. Concept of modular flexure-based mechanisms for ultra-high precision robot design. *Mech. Sci.* **2**, 99–107 (2011).
46. Correa, J. E., Toombs, J., Toombs, N. & Ferreira, P. M. Laminated micro-machine: Design and fabrication of a flexure-based Delta robot. *J. Manuf. Process.* **24**, 370–375 (2016).
47. Kalafat, M. A., Sevinç, H., Samankan, S., Altınkaynak, A. & Temel, Z. A Novel Origami-Inspired Delta Mechanism With Flat Parallelogram Joints. *J. Mech. Robot.* **13**, https://doi.org/10.1115/1.4048917 (2020).

48. Siskiyou MX7600. https://siskiyou.com/mx7600-series-manipulator/ (2025).
49. Sensapex uMP-3|4. https://shop.sensapex.com/product/ump-3/ (2025).
50. Motorized Micromanipulator SM 3.25. https://analyticaltechnologies.com.sg/products/accessories-supporting/micromanipulators/sm-3-25/ (2025).
51. PatchStar Micromanipulator. https://www.scientifica.uk.com/products/scientifica-patchstar-micromanipulator/technical-data (2025).
52. MP-285. https://www.sutter.com/MICROMANIPULATION/mp285.html (2025).
53. InjectMan® 4. https://www.eppendorf.com/ (2025).
54. M-VP-25XA-XYZL. https://www.newport.com/p/M-VP-25XA-XYZL (2025).
55. Mechonics MS15 xyz mounted. https://www.mechonics.de/products/positioners/ (2025).
56. Wu, T.-L., Chen, J.-H. & Chang, S.-H. A six-DOF prismatic-spherical-spherical parallel compliant nanopositioner. *IEEE Trans. Ultrason. Ferroelectr. Freq. Control* **55**, 2544–2551 (2008).
57. Zhang, R., Sherehiy, A., Wei, D. & Popa, D. O. Design and characterization of solid articulated four axes microrobot for microfactory applications. *J. Micro Bio Robot.* **15**, 119–131 (2019).
58. Cai, K. et al. Modeling and controller design of a 6-DOF precision positioning system. *Mech. Syst. Signal Process.* **104**, 536–555 (2018).
59. Ahn, D., Choi, Y.-M. & Jeong, J. Design of a four-degree-of-freedom nano positioner utilizing electromagnetic actuators and flexure mechanisms. *Rev. Sci. Instrum.* **86**, 035101 (2015).
60. Varadarajan, K. M. & Culpepper, M. L. A dual-purpose positioner-fixture for precision six-axis positioning and precision fixturing: Part II. Characterization and calibration. *Preci. Eng.* **31**, 287–292 (2007).
61. Furutani, K., Suzuki, M. & Kudoh, R. Nanometre-cutting machine using a stewart-platform parallel mechanism. *Mea. Sci.Technol.* **15**, 467 (2004).
62. Zhang, D. et al. Design and assessment of a 6-DOF Micro/Nanopositioning System. *IEEE/ASME Trans. Mechatron.* **24**, 2097–2107 (2019).
63. Feng, B., Liu, Y., Zhang, J., Qu, S. & Yang, W. Miniature origami robot for various biological micromanipulations. zenodo https://doi.org/10.5281/zenodo.14860767 (2025).

Acknowledgements

This work is supported by the National Natural Science Foundation of China (Nos. 12321002, 91748209, awarded to S.Q.) and 111 Project of China (No. B21034, awarded to S.Q.). We thank Prof. Xinjun Liu and Prof. Fugui Xie for their suggestions in parallel mechanism design. We thank Hejinsheng Cao and Ji Tang for their help in PCBs.

Author contributions

Y.L. and S.Q. developed the concept; B.F. and Y.L. build the robot; B.F., Y.L., and J.Z. conducted the experimental work; B.F., Y.L., and J.Z. contributed to modeling and data analysis; S.Q. and W.Y. supervised the project. All authors contributed to the paper writing.

Competing interests

The "split and splice" method described in this paper has been granted a patent in China (Author: Y.L., B.F, S.Q., Patent Number: [CN 202211568273.7]). In addition, we have initiated the PCT (Patent Cooperation Treaty) international patent application process (Application Number: [PCT/CN2023/079940]) and are in the planning stages of applying for a patent in the United States. The Micro-X4 micromanipulator described in this paper has been granted a patent in China (Author: Y.L., B.F., and S.Q., Patent Number: [CN 202310510732.4]). In addition, we have initiated the PCT international patent application process and are in the planning stages of applying for a patent in the United States. The authors declare no other competing interests.

Additional information

Supplementary information The online version contains supplementary material available at https://doi.org/10.1038/s41467-025-57815-5.

Correspondence and requests for materials should be addressed to Yide Liu or Shaoxing Qu.

Peer review information *Nature Communications* thanks Merve Acer Kalafat, Tuo Zhao, and the other anonymous reviewers for their contribution to the peer review of this work. A peer review file is available.